Low-Level Cloud Budgets across Sea Ice Edges

YOUTONG ZHENG[a] AND YI MING[b]

[a] *Program in Atmospheric and Oceanic Sciences, Princeton University, Princeton, New Jersey*
[b] *NOAA/Geophysical Fluid Dynamics Laboratory, Princeton, New Jersey*

(Manuscript received 26 April 2022, in final form 31 August 2022)

ABSTRACT: Interpreting behaviors of low-level clouds (LLCs) in a climate model is often not straightforward. This is particularly so over polar oceans where frozen and unfrozen surfaces coexist, with horizontal winds streaming across them, shaping LLCs. To add clarity to this interpretation issue, we conduct budget analyses of LLCs using a global atmosphere model with a fully prognostic cloud scheme. After substantiating the model's skill in reproducing observed LLCs, we use the modeled budgets of cloud fraction and water content to elucidate physics governing changes of LLCs across sea ice edges. Contrasting LLC regimes between open water and sea ice are found. LLCs over sea ice are primarily maintained by large-scale condensation: intermittent intrusions of maritime humid air and surface radiative cooling jointly sustain high relative humidity near the surface, forming extensive but tenuous stratus. This contrasts with the LLCs over open water where the convection and boundary layer condensation sustain the LLCs on top of deeper boundary layers. Such contrasting LLC regimes are influenced by the direction of horizontal advection. During on-ice flow, large-scale condensation dominates the regions, both open water and sea ice regions, forming clouds throughout the lowest several kilometers of the troposphere. During off-ice flow, as cold air masses travel over the open water, the cloud layer lifts and becomes denser, driven by increased surface fluxes that generate LLCs through boundary layer condensation and convective detrainment. These results hold in all seasons except summer when the atmosphere–surface decoupling substantially reduces the footprints of surface type changes.

KEYWORDS: Advection; Budgets; Climatology; Clouds; Arctic; Sea ice

1. Introduction

As the planet continues to warm, sea ice packs in the polar regions continue to shrink (Simmonds 2015; Stroeve et al. 2012). The loss of sea ice causes darker surfaces that absorb more incoming solar energy, amplifying the warming (Hall 2004; Manabe and Wetherald 1975). Moreover, the opening of sea ice packs significantly increases the surface fluxes of moisture and energy by removing the sea ice as an effective insulator (Taylor et al. 2018). This can moisten the boundary layer and create more and denser clouds, in particular in colder seasons when the stronger atmospheric radiative cooling favors upward transport of moisture from the ocean (Kay and Gettelman 2009). The finding of more and denser clouds due to melting sea ice in nonsummer seasons is confirmed by observations at different spatial–temporal scales (Wall et al. 2017; Morrison et al. 2018; Barton et al. 2012; Eastman and Warren 2010; Palm et al. 2010; Monroe et al. 2021; Taylor et al. 2015) and by some climate models (Wall et al. 2017; Kay and Gettelman 2009; Morrison et al. 2019). Despite the consensus on the qualitative behavior of cloud response to melting sea ice, the uncertainty of its representation in climate models remains large. For example, current climate models do not even agree on the sign of the Arctic cloud feedback in response to anthropogenic forcing (Zelinka et al. 2013; Pithan and Mauritsen 2014). This is not surprising given the complex interactions between clouds, radiation, sea ice, and large-scale circulation and the fact that subgrid-scale cloud processes are parameterized.

Understanding the statistics of clouds in a climate model is never straightforward. This is particularly the case for polar oceans that contain both ice-covered and open-water surfaces, with advection of air masses across them (Taylor et al. 2018; Tjernström et al. 2015; You et al. 2021; Woods et al. 2013). The circulation over the sea ice surfaces is usually dominated by anticyclones, but invasions of migratory cyclones are frequent (Herman and Johnson 1980; Curry et al. 1996). This changes low-level wind directions across the boundary of the two surface types, causing dramatically different regimes of low-level cloud (LLC). For example, when maritime air advects over the pack ice, layering of LLCs tends to emerge (Herman and Goody 1976; Cronin and Tziperman 2015; Cronin et al. 2017), whereas the opposite situation (air masses traveling from ice pack to open water) often invokes the LLC regime transition from layered stratus to cumuliform clouds (Geerts 2019). The former situation can double the mean cloudiness, perturbing the surface net longwave radiation by several tens of watts per meter squared ($W\ m^{-2}$) (Messori et al. 2018). Thus, understanding how changes in horizontal advection modify polar LLCs helps interpret their climatology and their radiative effects on polar climate.

Denotes content that is immediately available upon publication as open access.

Supplemental information related to this paper is available at the Journals Online website: https://doi.org/10.1175/JCLI-D-22-0301.s1.

Ming's current affiliation: Schiller Institute for Integrated Science and Society and Department of Earth and Environmental Sciences, Boston College, Boston, Massachusetts.

Corresponding author: Youtong Zheng, youtong.zheng@noaa.gov

DOI: 10.1175/JCLI-D-22-0301.1

© 2022 American Meteorological Society. For information regarding reuse of this content and general copyright information, consult the AMS Copyright Policy (www.ametsoc.org/PUBSReuseLicenses).

Unauthenticated | Downloaded 12/19/22 09:10 PM UTC

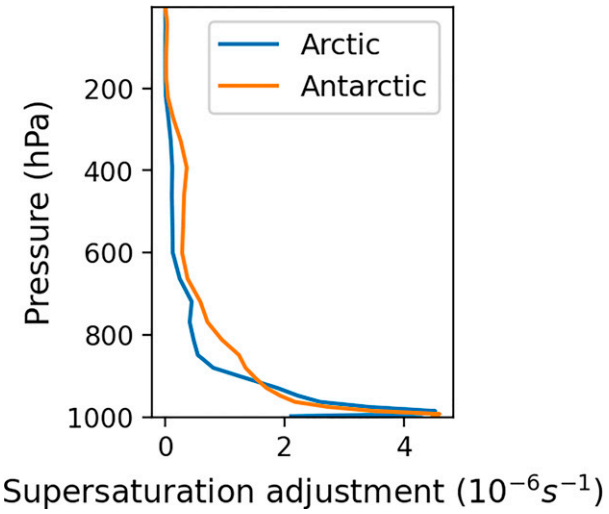


FIG. 1. Vertical profiles of $\partial a/\partial t|_{\text{super}}$ for the Arctic (70°–90°N) and Antarctic (70°–90°S).

Most prior studies of polar clouds using climate models, however, do not drill down to such process-level detail (Inoue et al. 2006; Vavrus 2004; Vavrus et al. 2008, 2011; Morrison et al. 2019; Hu et al. 2018; Kay and Gettelman 2009). One reason for the lack of process-level explorations is the lack of model diagnostics that explicitly explain the behaviors of LLCs. Commonly used diagnostics are mean-state variables such as relative humidity, lower-tropospheric stratification, and surface fluxes. These diagnostics, however, are merely environmental variables that may have a bearing on LLCs whereas representations of LLCs in a climate model are more complex. For example, lower-tropospheric stability (LTS) has been considered a good predictor of low-level cloudiness (Klein and Hartmann 1993; Wood and Bretherton 2006). The physics behind this diagnostic is that a larger LTS traps within the boundary layer moisture originating from the ocean, making more LLCs. To what degree this mechanism operates over frozen surfaces, however, is an open question because sea ice shuts off the influxes of moisture from the underlying ocean. This partially accounts for the markedly worse performance of LTS as a predictor of LLC cover over polar oceans than over subtropical and midlatitude oceans (Wood 2012; Yu et al. 2019).

To add clarity to the understanding of surface dependence of polar LLCs, we conduct process-oriented budget analyses of LLCs over polar oceans using the Geophysical Fluid Dynamics Fluid (GFDL) Atmospheric Model AM4.0 (Zhao et al. 2018). The GFDL AM4.0 employs prognostic schemes for both cloud water content and cloud fractional coverage,

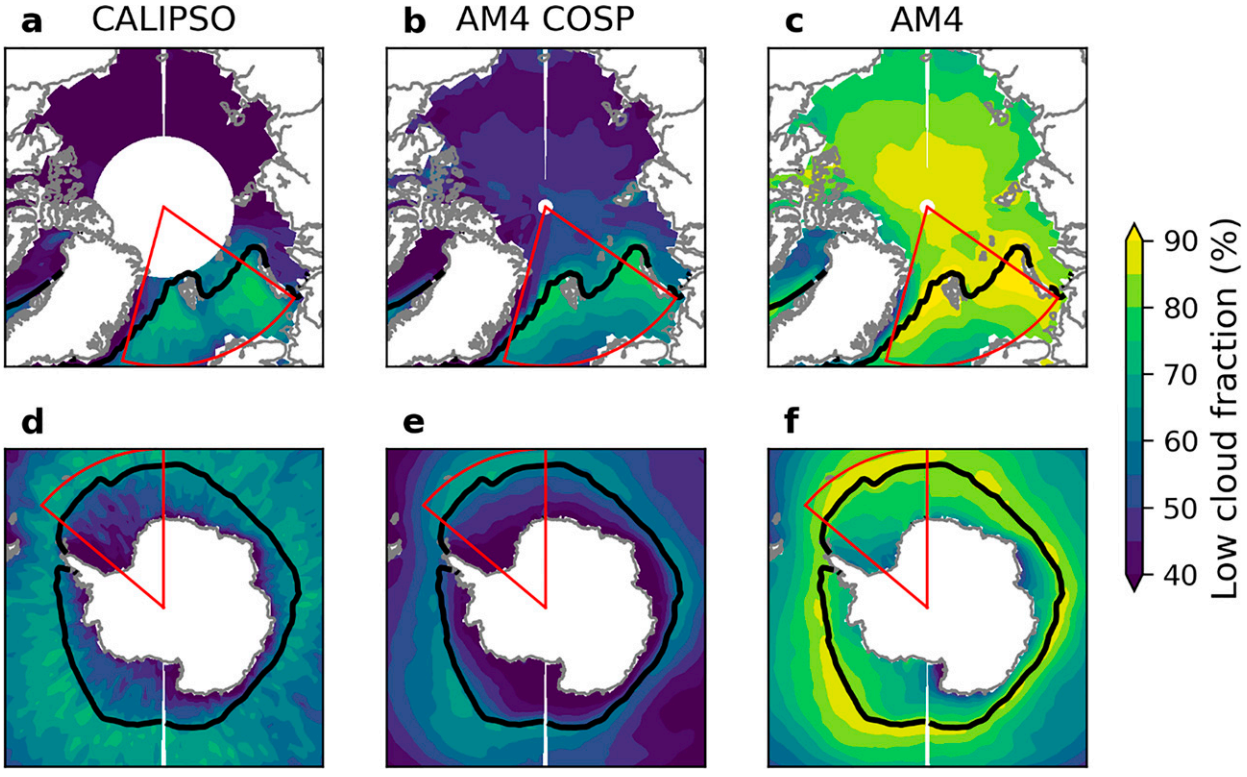


FIG. 2. Wintertime climatology (2006–14) of low cloud fraction over the (top) Arctic and (bottom) Antarctic oceans from (a),(d) *CALIPSO*-GOCCP observations, (b),(e) the AM4 model with *CALIPSO* simulator, and (c),(f) default AM4. The chosen winter months are December, January, and February for the Arctic and June, July, and August for the Antarctic. The black lines mark the sea ice edges defined as sea ice concentration of 50%. The red lines encompass regions of interest for transect plots, with continental data removed from the analysis.

Unauthenticated | Downloaded 12/19/22 09:10 PM UTC

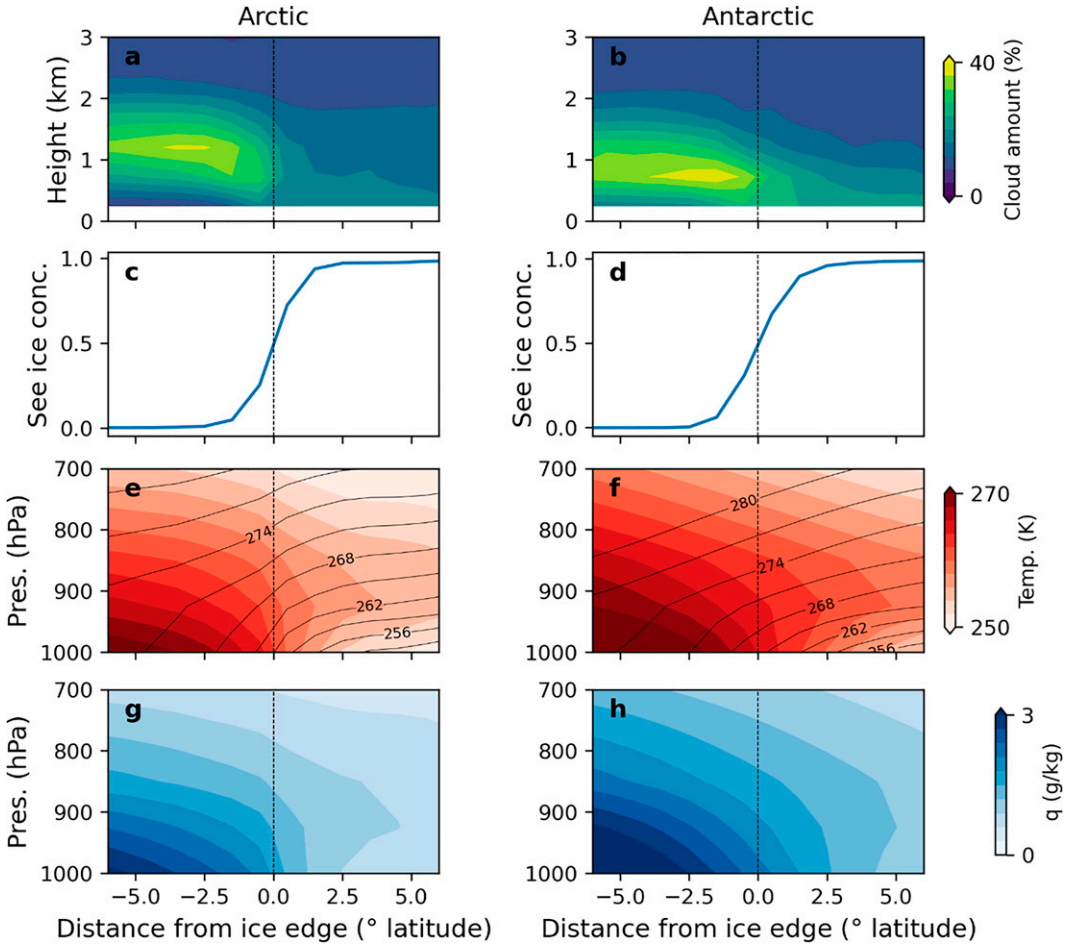


FIG. 3. Vertical profiles of (a),(b) *CALIPSO*-observed cloud fraction, reanalysis (e),(f) temperature and (g),(h) specific humidity, and (c),(d) sea ice concentration as a function of meridional distance from sea ice edges over (left) the Atlantic region of the Arctic and (right) the Weddell Sea in the Antarctic. In (e) and (f), the black contours mark the potential temperature.

allowing us to delve into the tendency terms that generate and dissipate the LLCs. Instead of looking at the entire polar region, we focus on the marginal sea ice region for two reasons. First, as already discussed, advections across sea ice edges are crucial *processes* governing polar LLCs. By focusing on LLCs associated with advection events, we can conduct process-oriented evaluations (Maloney et al. 2019) of the GFDL AM4.0, assessing whether the model reproduces the observations for the right reasons. Second, the sharp transition between sea ice and open water is a natural test bed for investigating the surface-type dependence of LLCs. This is highly relevant for understanding the polar low cloud feedback.

Our objective is twofold: 1) conducting process-oriented evaluations of the simulated LLC cloudiness by the GFDL AM4.0 against satellite observations in polar regions and 2) elucidating the physical mechanisms of LLC changes across sea ice edges by conducting budget analyses of LLCs. The next section introduces the GFDL AM4.0 and satellite observations. Section 3 presents the model evaluation results, showing that the GFDL AM4.0 does a satisfactory job of simulating polar LLCs. Section 4 shows results from the budget analyses, followed by the analysis examining the representativeness of the results in section 5. Discussions and conclusions are given in section 6.

2. Data and methodology

a. *GFDL AM4*

The Geophysical Fluid Dynamics Laboratory (GFDL) Atmospheric Model AM4.0 is the GFDL's latest atmosphere climate model (Zhao et al. 2018). It has a horizontal resolution of ~100 km, with 33 vertical model levels. It adopts the dynamic core from the hydrostatic version of the GFDL Finite-Volume Cubed-Sphere Dynamical Code (FV3; Lin 2004). AM4.0 uses a "double-plume" convective closure scheme to parameterize both shallow and deep convection (Zhao et al. 2018). The PBL scheme is based on Lock et al. (2000).

Unauthenticated | Downloaded 12/19/22 09:10 PM UTC

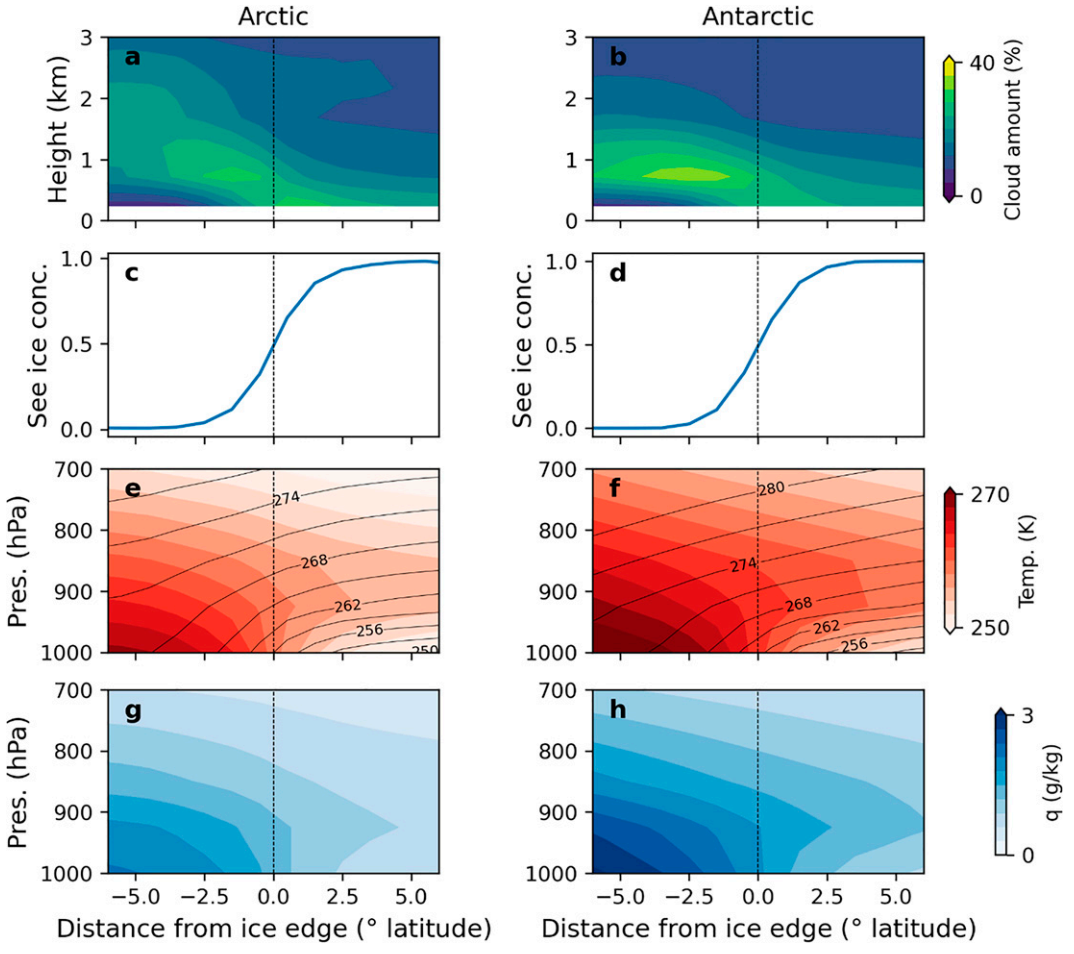


FIG. 4. As in Fig. 3, but for AM4 with *CALIPSO* simulator.

The cloud microphysics scheme is a one-moment bulk scheme that is primarily based on the works of Rotstayn (1997) and Jakob and Klein (2000). This scheme has two limitations. First, compared with the more sophisticated two-momentum scheme with prognostic precipitation (Morrison and Gettelman 2008; Gettelman and Morrison 2015), the scheme removes too much cloud water, contributing to the underestimation of subtropical coastal stratocumulus (Guo et al. 2021). Second, the scheme tends to overestimate the ice cloud fraction, partially due to the poorly constrained parameterization of ice nucleation (Guo et al. 2021).

The AM4.0 uses a model-consistent prognostic cloud macrophysical scheme developed by Tiedtke (1993). The scheme parameterizes the cloud fraction (a) and cloud liquid water content (l) prognostically:

$$\frac{\partial a}{\partial t} = \underbrace{\left.\frac{\partial a}{\partial t}\right|_{\text{ad}}}_{\text{advection}} + \underbrace{\left.\frac{\partial a}{\partial t}\right|_{\text{cv}}}_{\text{convection}} + \underbrace{\left.\frac{\partial a}{\partial t}\right|_{\text{ls-cond}}}_{\text{large-scale condensation}} + \underbrace{\left.\frac{\partial a}{\partial t}\right|_{\text{er}}}_{\text{erosion}} + \underbrace{\left.\frac{\partial a}{\partial t}\right|_{\text{vd}}}_{\text{vertical diffusion}} + \underbrace{\left.\frac{\partial a}{\partial t}\right|_{\text{super}}}_{\text{supersaturation adjustment}}, \quad (1)$$

$$\frac{\partial l}{\partial t} = \underbrace{\left.\frac{\partial l}{\partial t}\right|_{\text{ad}}}_{\text{advection}} + \underbrace{\left.\frac{\partial l}{\partial t}\right|_{\text{cv}}}_{\text{convection}} + \underbrace{\left.\frac{\partial l}{\partial t}\right|_{\text{ls-cond}}}_{\text{large-scale condensation}} + \underbrace{\left.\frac{\partial l}{\partial t}\right|_{\text{er}}}_{\text{erosion}} + \underbrace{\left.\frac{\partial l}{\partial t}\right|_{\text{vd}}}_{\text{vertical diffusion}} + \underbrace{\left.\frac{\partial l}{\partial t}\right|_{\text{super}}}_{\text{supersaturation adjustment}} + \underbrace{\left.\frac{\partial l}{\partial t}\right|_{\text{ev}}}_{\text{evaporation}} + \underbrace{\left.\frac{\partial l}{\partial t}\right|_{\text{micro}}}_{\text{microphysical processes}}, \quad (2)$$

in which the physical meaning of each term is described underneath.

In both budget equations, the advection, convection, and vertical diffusion terms are determined in model modules of dynamics, convection, and planetary boundary layer, respectively. In Eq. (1), the large-scale condensation and erosion terms are computed by Tiedtke's parameterization with some modifications (Anderson et al. 2004). In Eq. (2), the large-scale condensation term is determined as the rate at which the saturation specific humidity decrease over time, which primarily depends on the strength of large-scale lifting and diabatic cooling.

Unauthenticated | Downloaded 12/19/22 09:10 PM UTC

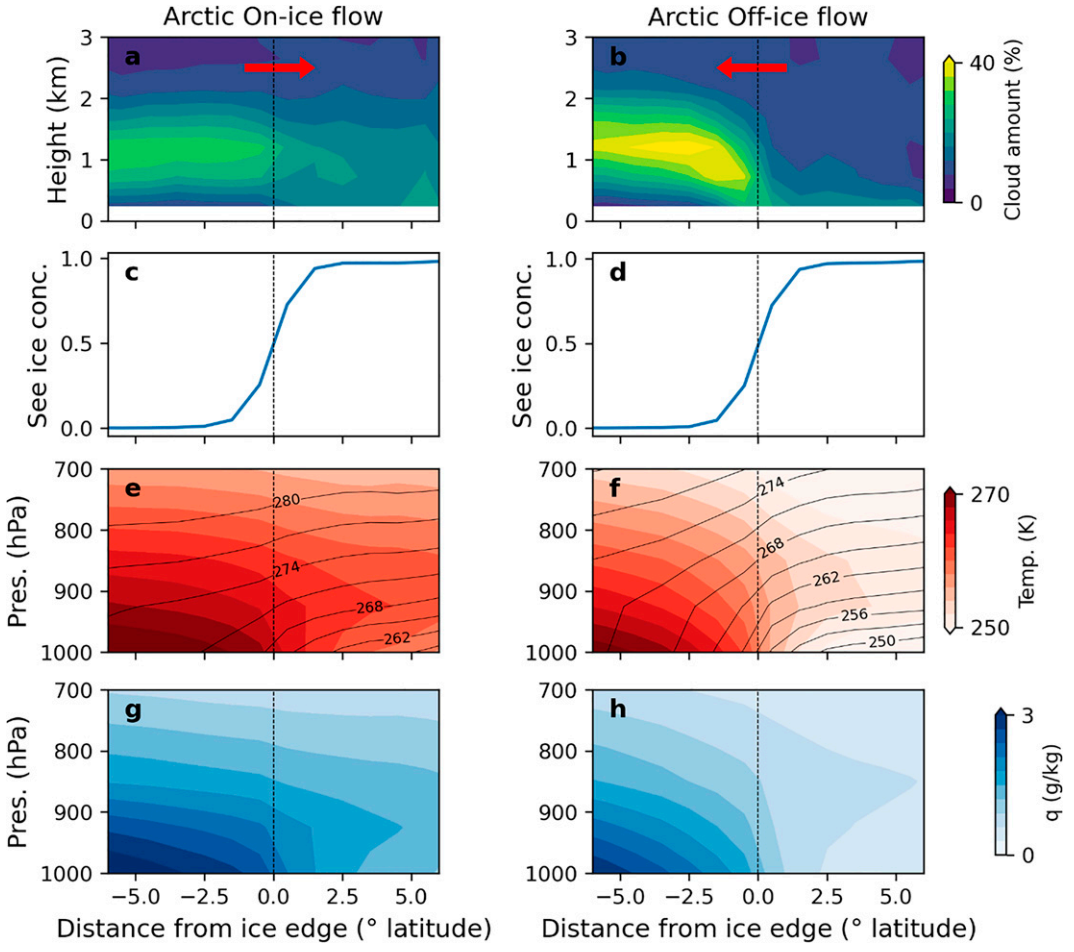


FIG. 5. As in Fig. 3, but for (left) on-ice and (right) off-ice flow conditions in the Arctic. The on-ice and off-ice flow days are defined as days with the meridional surface wind speed near the ice edge larger than 3 m s^{-1} and smaller than −3 m s^{-1}, respectively.

Equation (2) has two additional terms. The first is the evaporation term, $\partial l/\partial t|_{ev}$, which refers to the evaporation of cloud droplets by large-scale subsidence and warming. Note that this is different from the erosion that refers to the horizontal turbulent mixing between saturated and unsaturated air. The second is the microphysics term, $\partial l/\partial t|_{micro}$, which includes the autoconversion, accretion, freezing, riming, and Bergeron–Findeisen processes. The net effect of these processes is to consume cloud liquid water.

The interpretation of the supersaturation adjustment term merits discussions here. This term removes any vapor in excess of supersaturation by condensing it into the cloud. The mean vertical profiles of $\partial a/\partial t|_{super}$ over the Arctic and Antarctic show distinctive bottom-heavy structures (Fig. 1), with peaks in the boundary layer. The peaks are primarily due to the moistening by the turbulent flux of moisture in the boundary layer. This argument can be explained as follows. In the free atmosphere, if the grid-averaged relative humidity is larger than a threshold value, large-scale condensation will initiate as long as the saturation specific humidity (q_s) decreases with time (i.e., $dq_s/dt < 0$), typically caused by large-scale lifting or diabatic cooling. The large-scale condensation helps remove water vapor from the atmosphere, limiting the occurrence of supersaturation. Thus, this term is typically a small one, compared with other terms in Eq. (1). Supersaturation, however, might happen if the vapor-removing rate (dq_s/dt) is slower than the rate of moistening. This is most likely to happen in the boundary layer of a subsiding atmosphere, such as polar regions, where the subsidence-induced warming substantially buffers the temporal decrease of q_s, but the surface moisture flux moistens the boundary layer in a more rapid rate. Based on this argument, the physical meaning of the supersaturation adjustment term in polar regions can be considered a portion of the boundary layer condensation. Such a physical interpretation helps us distinguish between the large-scale condensation term and the supersaturation term, with the former manifesting at the grid-mean scale and the latter at subgrid scale.

The simulation conducted in this study is the same as the standard Atmospheric Model Intercomparison Project (AMIP) simulation (Zhao et al. 2018). The sea surface temperature and sea ice concentration and thickness are prescribed. For the evaluation purpose, we extract the model output from 2006 to 2014

Unauthenticated | Downloaded 12/19/22 09:10 PM UTC

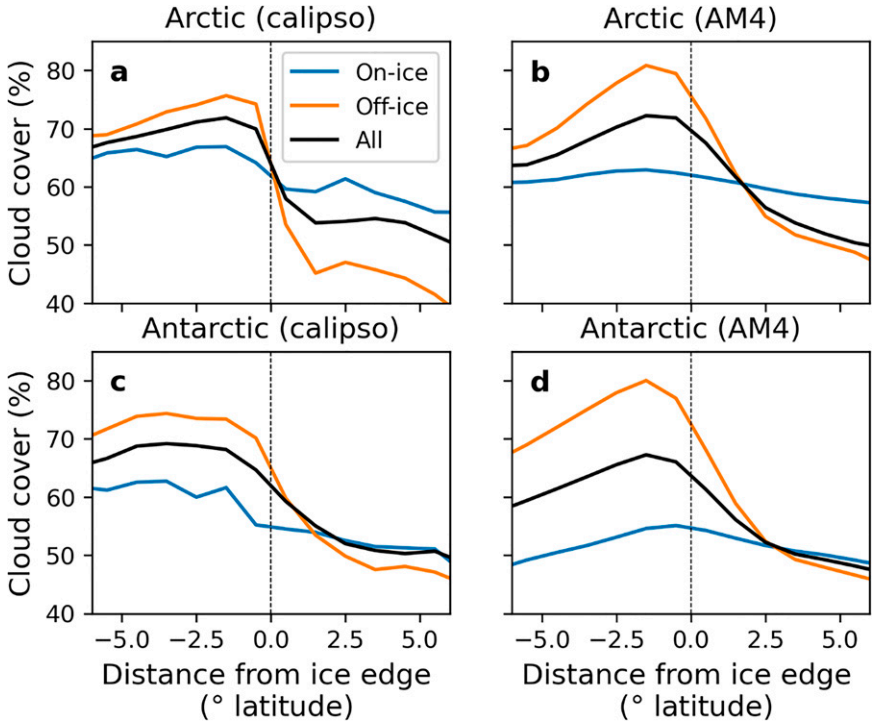


FIG. 6. Low cloud fraction as a function of the meridional distance from sea ice edges for (a),(c) *CALIPSO* and (b),(d) AM4 with *CALIPSO* simulator over the (top) Arctic and (bottom) Antarctic.

to match the period when the *Cloud–Aerosol Lidar and Infrared Pathfinder Satellite Observations* (*CALIPSO*) observations are available. We use the daily output for analyses of temperature advection influences on LLCs (i.e., on-ice versus off-ice flows). Due to the sheer volume of daily three-dimensional tendency terms, we only use the data between 2010 and 2014 for budget analyses. Selecting different periods does not change the conclusions.

b. *Satellite observations*

We use the data from the Cloud–Aerosol Lidar with Orthogonal Polarization (CALIOP) instrument onboard the *CALIPSO* satellite (Stephens et al. 2017). CALIOP is a lidar that measures profiles of backscatter. As an active instrument, the CALIOP overcomes two long-time issues of high-latitude cloud retrievals by traditional passive satellite sensors: 1) degradation of retrievals under high solar zenith angles and 2) unreliable cloud detections overlying bright surfaces. A caveat of CALIOP cloud retrieval is that the lidar beam is fully attenuated when the optical depth is greater than 3 (Winker et al. 2007), which causes the CALIOP to miss the bottom portion of low clouds. Among the various versions of *CALIPSO* products, we use the cloud fraction product from the General Circulation Model-Oriented *CALIPSO* Cloud Product (*CALIPSO*-GOCCP; Chepfer et al. 2010). The product has grid sizes of 1° in the horizontal and 480 m in the vertical. Within each 1° × 1° grid box, the cloud fraction is defined as the number of cloudy scenes divided by the total number of scenes without full attenuation of lidar beams. The LLCs are defined as clouds below 3.2 km.

We use the sea ice concentration data from the National Oceanic and Atmospheric Administration (NOAA)/National Snow and Ice Data Center (NSIDC) Climate Data Record of Passive Microwave Sea Ice Concentration dataset (Peng et al. 2013).

Whenever the satellite data are used, we focus on winter only. The main reason is that the *CALIPSO*-GOCCP data only cover regions equatorward of 80°N where the sea ice cover is most extensive in winter. As will become obvious later, one region of focus in this study is the Atlantic Ocean part of the Arctic where only during winter are there sufficient samples over sea ice.

Reanalysis data of temperature and humidity from the National Centers for Environmental Prediction (Kalnay et al. 1996) are used to complement the satellite data analysis.

3. Model evaluation

Figure 2 compares the AM4-simulated wintertime LLC cloud fraction with the *CALIPSO* observations (2006–14) over the Arctic and Antarctic ocean waters. Sea ice edges (defined as sea ice concentration of 50%) are marked by the black lines. *CALIPSO* shows considerably smaller cloudiness over ice packs than over the open oceans (Figs. 2a,d), consistent with observations reported in previous works (Morrison et al. 2018; Wall et al. 2017). Such a contrast in LLC cloud fraction between sea ice and open water is well reproduced by the AM4 with the *CALIPSO* simulator (Figs. 2b,e) although

Unauthenticated | Downloaded 12/19/22 09:10 PM UTC

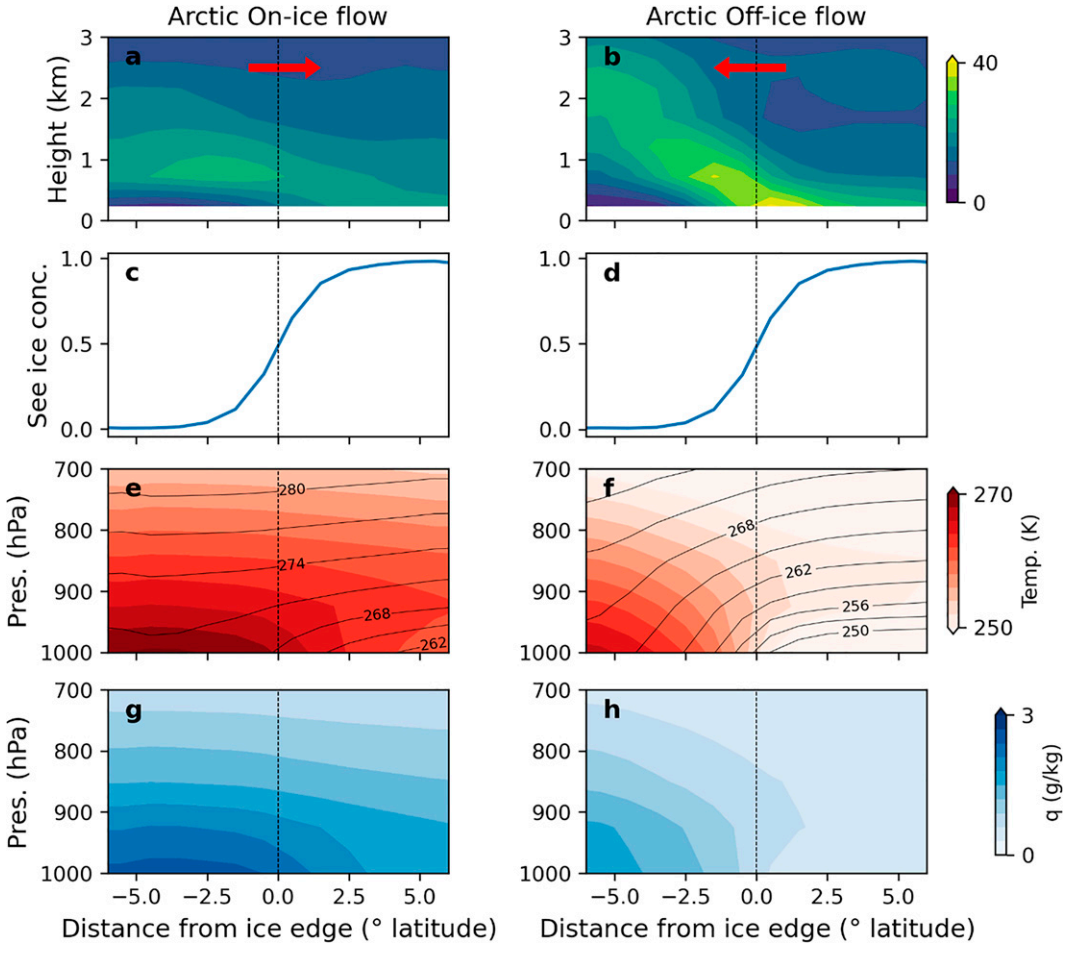


FIG. 7. As in Fig. 5, but for AM4 with *CALIPSO* simulator.

biases still exist such as overestimated and underestimated cloudiness over sea ice packs in Arctic and Antarctic regions, respectively.

Without the satellite simulator, the contrasting LLC cloud fraction between frozen and unfrozen surfaces becomes less distinctive in the Antarctic (Fig. 2f) and almost disappears in the Arctic (Fig. 2c). This is likely because LLCs over sea ice packs are so thin (Curry et al. 1996) that a large portion of them are undetected by *CALIPSO*.

Not only the total cloudiness of LLC but also its vertical distribution is important. To profile the clouds, we select two regions with stark transitions of sea ice concentration between open water and sea ice: the Atlantic region of the Arctic and the Weddell Sea of the Antarctic (areas encompassed by red solid lines in Fig. 2). We bin the data points according to their meridional distances to sea ice edges (Wall et al. 2017). This enables visualizing the vertical transects of cloudiness across the sea ice edges, shown in Fig. 3. The transect plots of *CALIPSO*-observed cloudiness exhibit substantial changes in the vertical structure of cloud fraction across the sea ice edges. Over the open water, the cloudiness maximizes near ~1 km, a typical height for marine planetary boundary layer (PBL) height, suggesting a commonly known cloud-topped marine PBL (LeMone et al. 2019). Moving from open water to ice packs, the height of maximum cloudiness declines to a level close to the surface. The maximum cloudiness also decreases considerably. Along with the changes in cloudiness are the changes in atmospheric sounding: a drier and more stable lower troposphere exists over ice packs than over open water. Such observed contrasts in the cloud vertical structure and atmospheric sounding across the sea ice edges are reasonably captured by the AM4 (Fig. 4) despite the existence of biases such as the underestimated cloudiness over the open water.

In addition to looking at the climatological mean, we examine key physical processes on shorter time scales to ensure that the model replicates the observations for the right reasons (Maloney et al. 2019). To that end, we use daily *CALIPSO* data to select two subsets: on-ice flow days and off-ice flow days. The criterion is based on the meridional wind speed averaged over a 4° distance centered on the sea ice edges, marked as v_{edge}. The PDF of v_{edge} exhibits roughly normal distribution with slightly positive skewness toward the positive end (not shown). We select the on-ice and off-ice days with $v_{\text{edge}} > 3\ \text{m s}^{-1}$ (on ice) or $< -3\ \text{m s}^{-1}$ (off ice), which follows

Unauthenticated | Downloaded 12/19/22 09:10 PM UTC

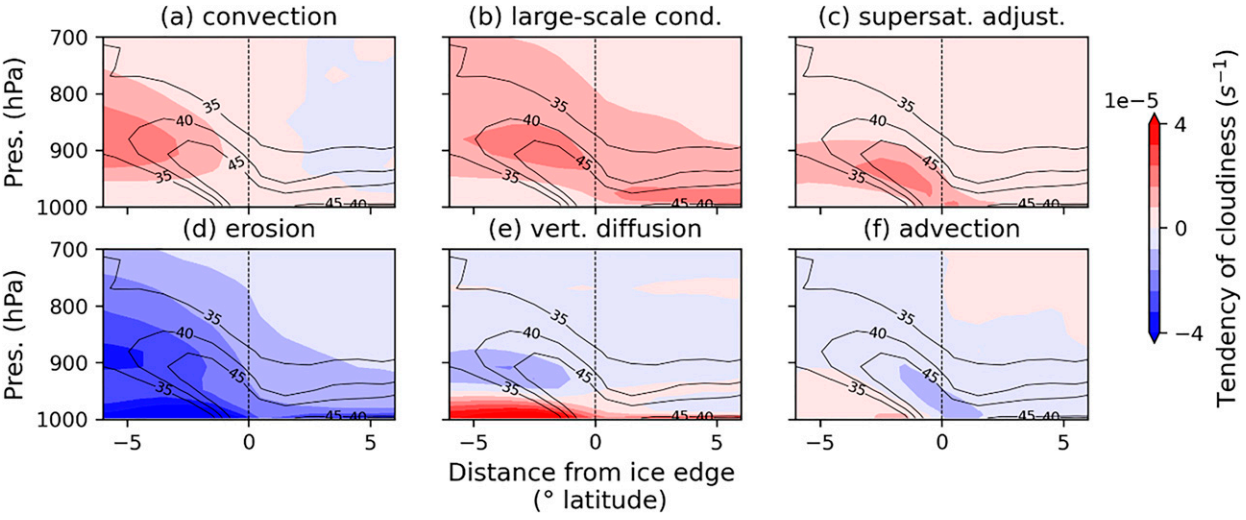


FIG. 8. Vertical transects of tendencies of cloud fraction in the winter. Black contours mark the cloud fraction (with no satellite simulator).

Wall et al. (2017). The on-ice and off-ice days occupy 15% and 27% of the total days, respectively in the Arctic (17% and 19% for the Antarctic). The conclusions are not sensitive to the threshold of v_{edge}. The u-wind component is not considered because its influence on the results was found to be small (see Figs. S2–S5 in the online supplemental material).

Before examining the results for on- and off-ice composites, we bring up an important point: compositing cases for fixed wind direction allows interpreting the results from the Lagrangian perspective (Schubert et al. 1979; Chung et al. 2012). Given a variable A in a one-dimensional space, the climatological averaging yields $\partial\overline{A}/\partial t = 0$, leading to $d\overline{A}/dt = \overline{V}(\partial\overline{A}/\partial x)$, in which $\overline{V}$ is the climatological mean wind speed. If the wind does not change, the $\partial\overline{A}/\partial x$ can be interpreted in the Lagrangian sense of $d\overline{A}/dt$. This concept has long been used to interpret the subtropical stratocumulus-to-cumulus transitions from observations (Klein and Hartmann 1993; Zhou et al. 2015; Zheng et al. 2018).

Figure 5 shows the transect plots for on- and off-ice composites in the Atlantic part of the Arctic. Stark differences between the two situations are found. During on-ice flow, warm and humid air from the open water intrudes into a drier and colder environment over the sea ice packs, warming and moistening the region. The maritime humid air cools by radiation and diffusion, bringing the air to saturation, creating clouds throughout the lowest ~2 km over the ice packs, a typical consequence of warm and humid air intrusion (Herman and Goody 1976; Curry 1983). During off-ice flow, however, the air column over the sea ice is drier, colder, and less cloudy. The clouds are more confined near the ice surface. As the cold airstreams over the warm ocean, the lower troposphere destabilizes (Fig. 5f) and the cloud layer lifts (Fig. 5b), characteristic of cold air outbreaks.

The influence of advection can be more clearly seen in the left panels of Fig. 6 showing the total fractional coverage of LLCs over both regions. The on-ice flow suppresses low clouds over open water but generates more clouds over sea ice. The opposite is true for off-ice flow.

The observed advection dependence of LLCs is reasonably simulated by the AM4 (Figs. 6 and 7). The AM4 succeeds in simulating the following observed characteristics of LLCs across sea ice edges:

1) cloud structure changes typical of warm moist air intrusion (left panel of Fig. 7),
2) cloud structure changes typical of cold air outbreaks (right panel of Fig. 7), and
3) changes of LLC total cloudiness under on- and off-ice flow conditions (Fig. 6).

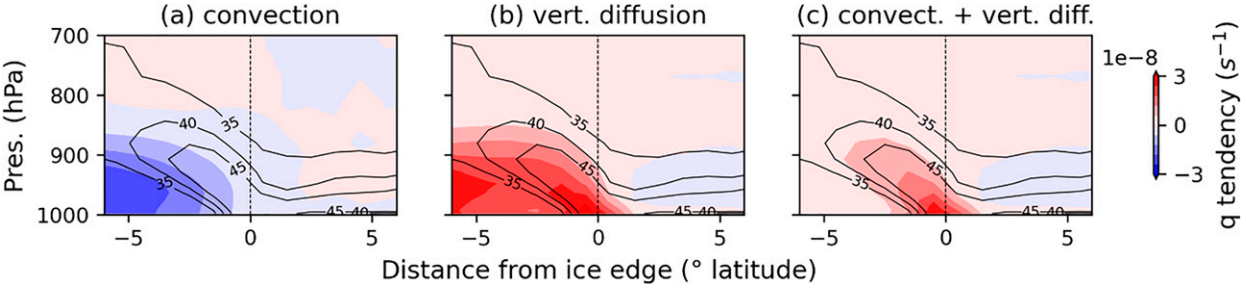


FIG. 9. Vertical transects of tendencies of specific humidity in the winter: (a) convection, (b) vertical diffusion, and (c) convection plus vertical diffusion. Black contours mark the cloud fraction.

Unauthenticated | Downloaded 12/19/22 09:10 PM UTC

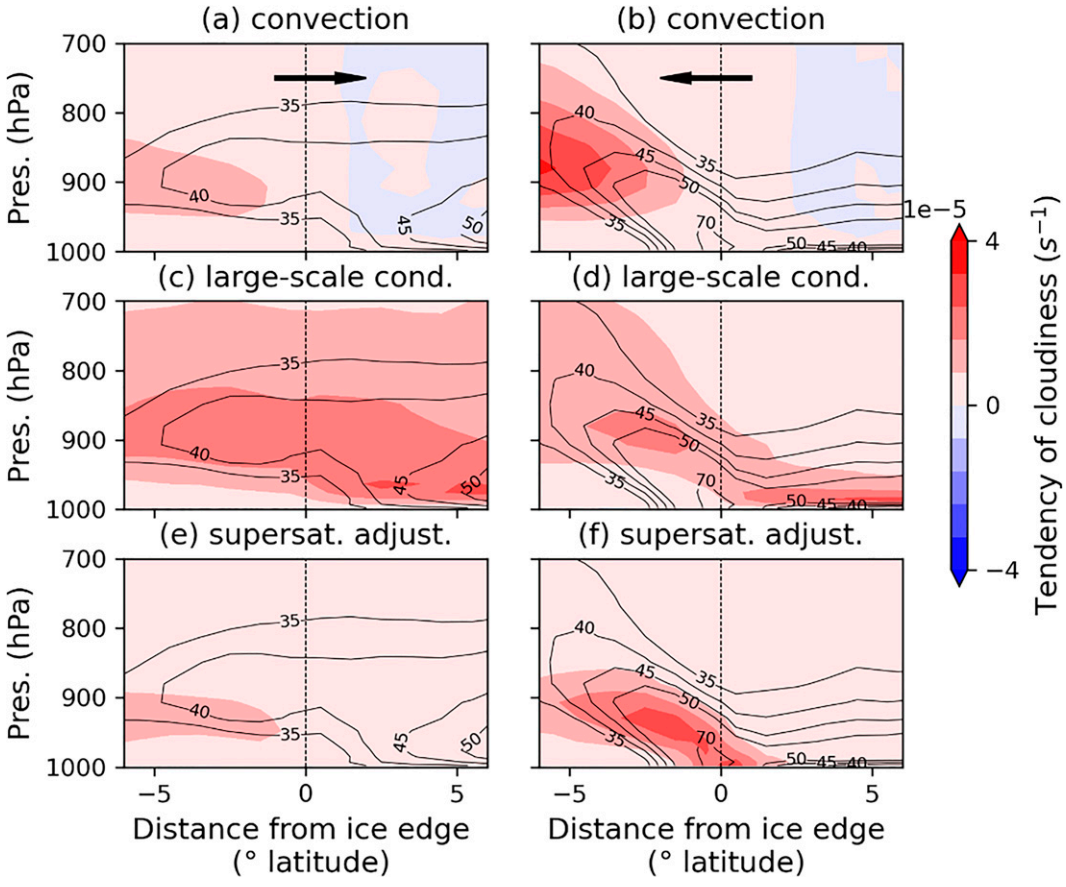


FIG. 10. Vertical transects of tendencies of sources of cloud fraction for (left) on-ice and (right) off-ice flow.

4. Budget analyses

Having demonstrated the fidelity of AM4's representation of the polar LLCs, we use the model to answer a couple of important scientific questions. What determines the climatological difference of LLCs between open water and sea ice? What controls the formations of LLCs when they are advected across the sea ice edges? Are these findings seasonally dependent? Although one might partially infer the answers from the last section, the questions cannot be fully answered without drilling down into the detail of the cloud budgets. Sections 4a and 4b focus on the budgets of cloud fraction and cloud liquid water content, respectively, which combine to answer the first two questions. Section 4c addresses the third question. We did not analyze the cloud ice water budget because over the region of interest, lower atmosphere near the ice edges, the clouds are primarily in liquid phase (Fig. S1). The predominance of liquid clouds seems surprising, especially on the sea ice side in winter. But given the fact that the LLCs over sea ice are trapped below 1 km where the air temperature is higher than −20°C, the supercooled liquid clouds are expected to predominate according to satellite observations (Hong and Liu 2015; Guo et al. 2020). It is encouraging that the AM4 captures this feature (Fig. S1) despite the limitations of the one-moment cloud microphysics scheme (Guo et al. 2021), as discussed in section 2. For compactness of presentation, we only show results from the Arctic region. The results hold for the Antarctic (see Figs. S6–S9).

a. Budgets of cloud fraction

Figure 8 shows the mean climatology of cloud fraction budgets in the Arctic winter. Overall, the erosion-induced cloud dissipation balances the cloud-producing processes of convective detrainment, large-scale condensation, and supersaturation adjustment. The advection and vertical diffusion redistribute the cloud fraction. Near the surface, there is a marked source of cloud fraction by vertical diffusion, counteracted by the strong erosion. Such a balance is realized via the dependence of erosion strength on the turbulence intensity in the model[1]: the more turbulent the fluid, the more strongly condensates mix with the ambient air.

The three cloud-generating terms (Figs. 8a–c) reveal different regimes of cloud formations in different regions: sea ice region ($x > \sim 2°$), ice-to-open-water transitional region ($\sim -2 < x < \sim 2°$), and open water region ($x < \sim -2°$). Over

[1] In the AM4, the erosion constant, a key parameter that governs the rate of erosion in Tiedtke's (1993) parameterization, is set to a larger value when the vertical diffusion is more active.

Unauthenticated | Downloaded 12/19/22 09:10 PM UTC

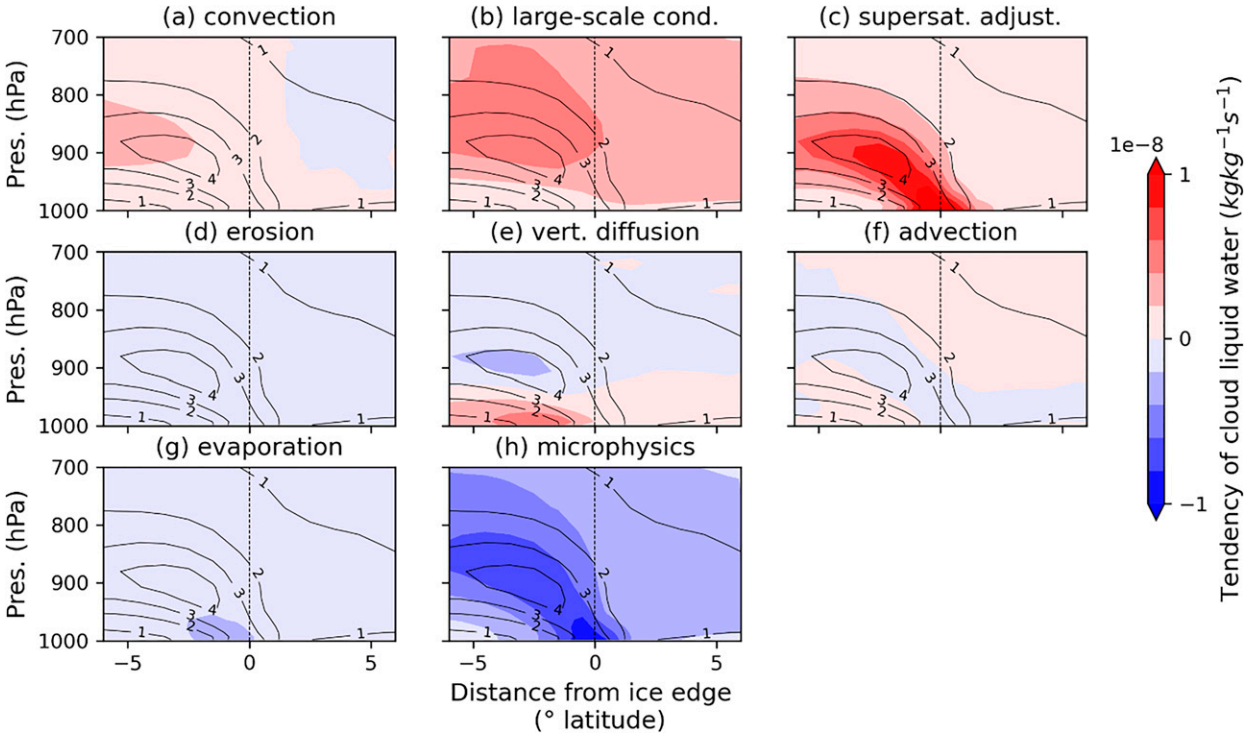


FIG. 11. Vertical transects of tendencies of cloud liquid water content scheme. Black contours mark the cloud total water content with values of 0.01, 0.02, 0.03, and 0.04 g kg^{-1}.

the sea ice, the low-lying clouds are dominantly formed by large-scale condensation that, to the first order, is determined by the relative humidity in AM4. The high relative humidity near the surface of sea ice is primarily maintained by the strong surface radiative cooling that 1) lowers the saturation vapor pressure and 2) sustains the near-surface temperature inversion that inhibits vertical diffusion of moisture. Note that there is no local source of moisture from the surface (Fig. 9b). The specific humidity over the sea ice likely originated from the intermittent intrusions of moist air from lower latitudes.

In the transitional region, the supersaturation adjustment adds to the source of cloud fraction. As a reminder, the condensation by supersaturation adjustment in polar boundary layers is primarily contributed by the boundary layer condensation (see discussion in section 2a). The enhanced supersaturation adjustment is driven by the influxes of moisture from the increasingly opened water. The moisture supplied from the surface is trapped within the boundary layer by the capping temperature inversion that, although weakened by the enhanced surface fluxes, is large enough to accumulate moisture and generate stratiform clouds. This can be more clearly seen from the transects of specific humidity budget terms $\partial q/\partial t|_{\mathrm{cv}}$ and $\partial q/\partial t|_{\mathrm{vd}}$ (Figs. 9a,b), in which the subscripts "cv" and "vd" represent convection and vertical diffusion, respectively. The $\partial q/\partial t|_{\mathrm{vd}}$ increases rapidly from the full sea ice region to the transitional region, moistening the boundary layer. This moistening effect is partly compensated by the drying effect of $\partial q/\partial t|_{\mathrm{cv}}$, which is still weak in the transitional region. As a result, there is a net moistening of the PBL (Fig. 9c), explaining the large contribution of supersaturation adjustment to the cloud fraction.

Over the open water, convective detrainment takes over as the dominant source, caused by the strong surface forcing. The strong convection also dries the subcloud layer, counteracting the moistening by vertical diffusion (Fig. 9), which lowers the boundary layer condensation (Fig. 8c).

The budgets differ substantially between on-ice and off-ice composites (Fig. 10). During on-ice flow, large-scale condensation is the leading source term throughout the entire region. This is consistent with the enhanced condensation when warm and moist air masses enter a colder environment (Curry 1983; Cronin and Tziperman 2015). The contributions from convection and supersaturation adjustment are smaller because of the warm-advection-induced stabilization of the lower troposphere suppresses the energy and moisture influxes from the ocean surface (Zheng and Li 2019; Zheng et al. 2020).

Under off-ice flow conditions, the dominance of large-scale condensation is replaced by supersaturation adjustment in the transitional region and by the convective detrainment over the open water (Fig. 10, right panel). The cold air masses experience two main stages when traveling over the open water. In the first stage, the gradually opened sea ice enhances the supply of moisture and energy from the ocean into the atmosphere (Fig. 16d). This destabilizes and deepens the boundary layer, gradually eroding the capping temperature inversion (Bretherton and Wyant 1997). The temperature inversion, although weakened, is still strong enough to trap the added

Unauthenticated | Downloaded 12/19/22 09:10 PM UTC

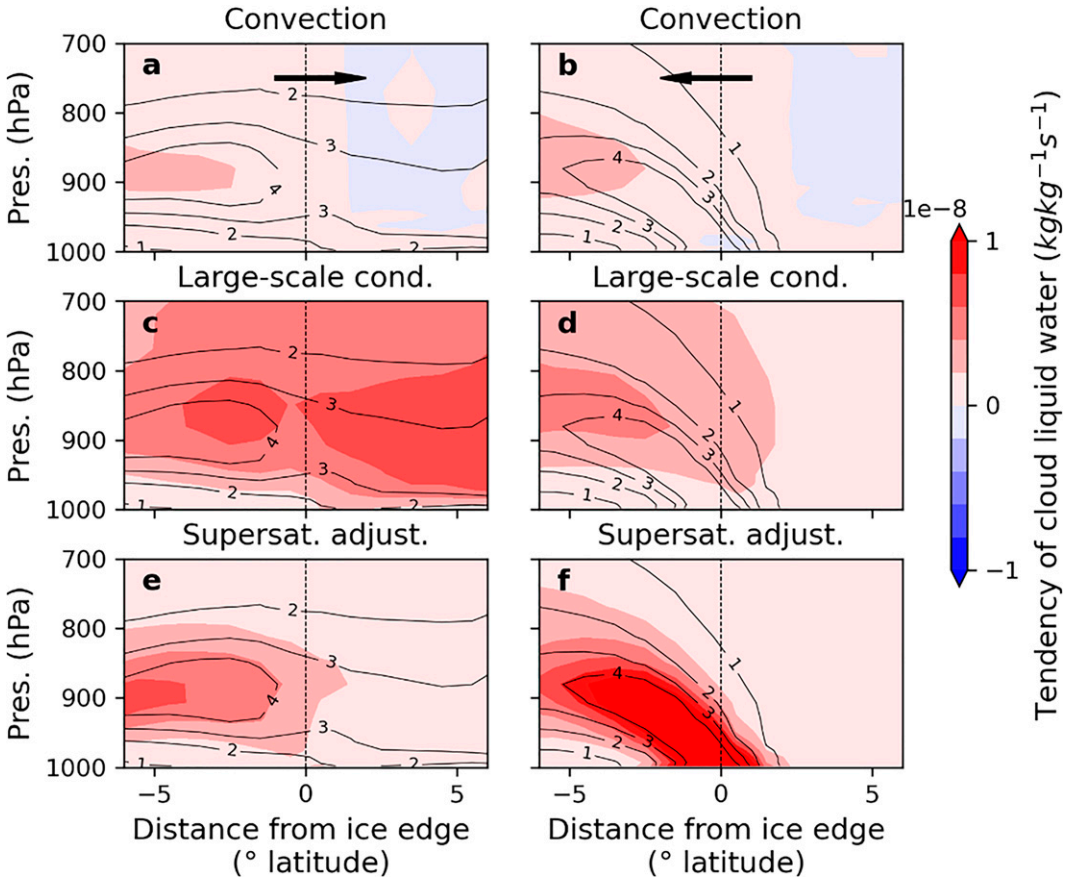


FIG. 12. As in Fig. 10, but for cloud liquid water content budgets. Black contours mark the cloud liquid water content with values of 0.01, 0.02, 0.03, and 0.04 g kg^{-1}.

moisture from the surface, forming LLCs. This explains the dominant source of supersaturation adjustment in the transitional region. In the second stage, as the lower atmosphere becomes more unstable, convection becomes increasingly active. The enhanced convection, on one hand, dries the boundary layer to dissipate the boundary layer stratus, and, on the other hand, generates more convective clouds that eventually dominate the cloud regime.

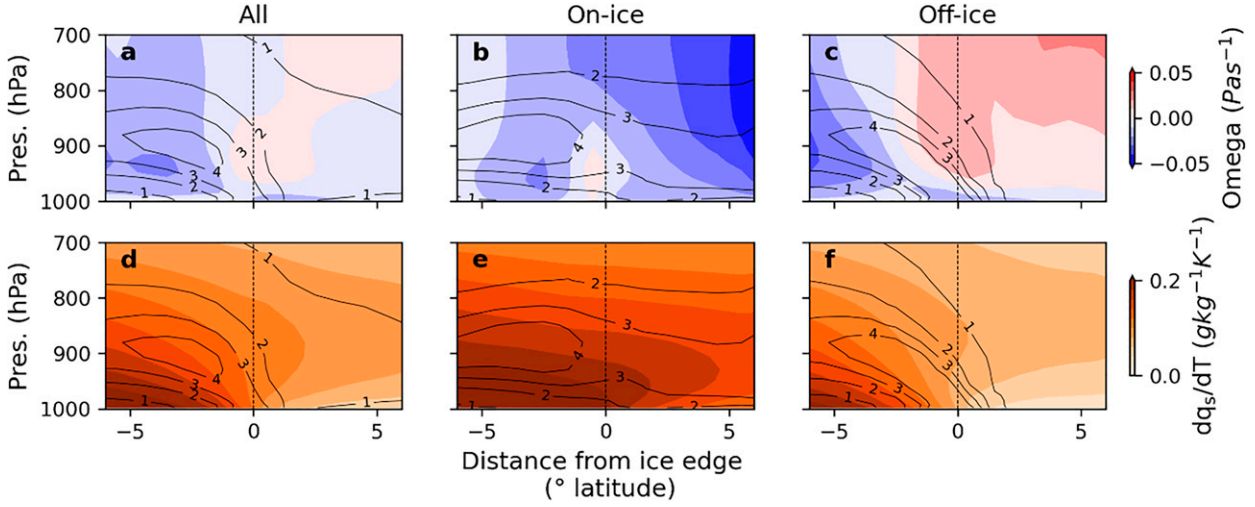


FIG. 13. Vertical transects of ω and dq_s/dT for (left) mean climatology and (center) on-ice and (right) off-ice flow conditions.

Unauthenticated | Downloaded 12/19/22 09:10 PM UTC

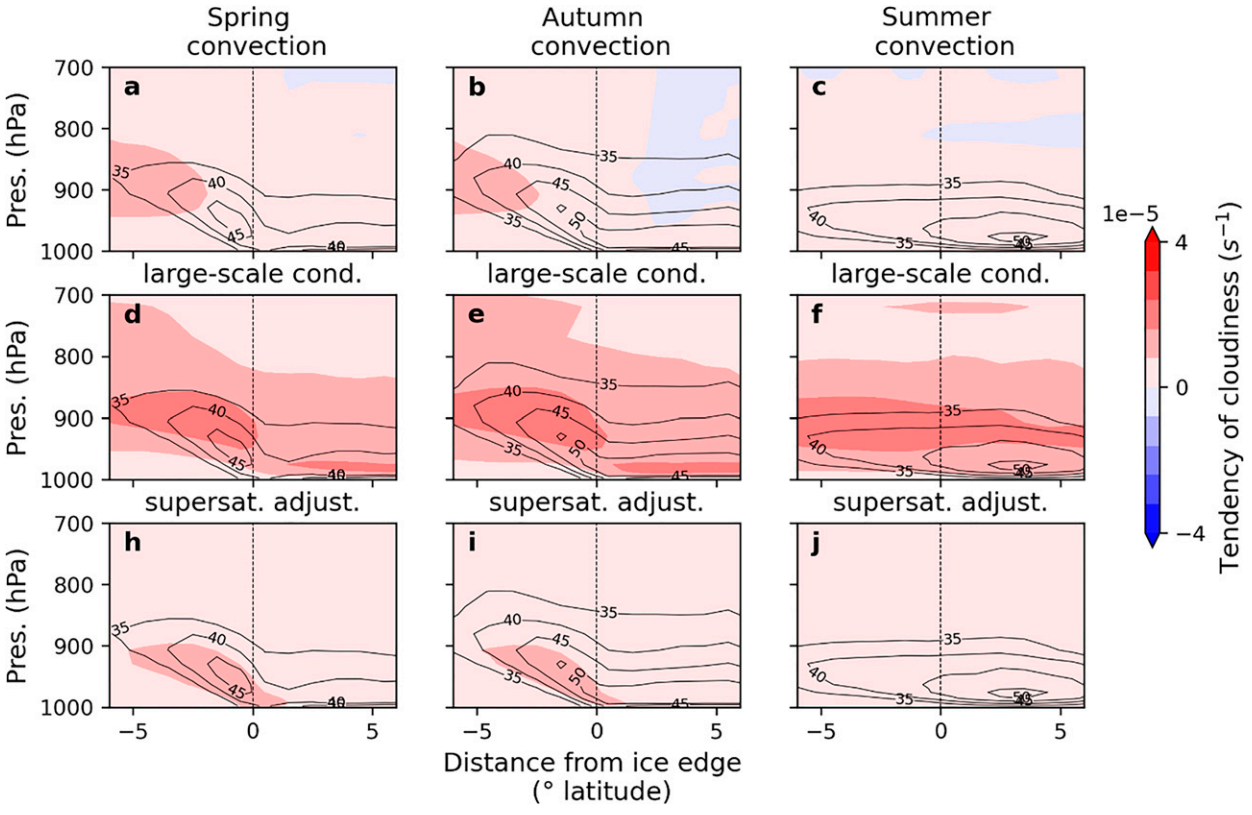


FIG. 14. As in Fig. 10, but for different seasons: (left) spring, (center) autumn, and (right) summer.

b. *Budgets of cloud liquid water content*

The cloud liquid water content (l) budgets (Figs. 11 and 12) show a similar picture with the cloud fraction budgets except for two aspects. First, the microphysical processes (i.e., depletion of cloud water by precipitation), rather than erosion, are the main sink term. This is expected. Second, the local maximum of large-scale condensation near the sea ice surface disappears. This phenomenon can be explained by the different ways that the large-scale condensation process is represented in the schemes of cloud fraction and l. Unlike the cloud fraction scheme in which the large-scale condensation is mainly determined by relative humidity, the l is more sensitive to the rate at which the saturation specific humidity (q_s) decreases over time:

$$dq_s/dt = dq_s/dp(\omega + gM_c) + dq_s/dT(dT/dt), \qquad (3)$$

in which the ω is the large-scale vertical velocity, gM_c represents the subsidence forced by cumulus mass flux (M_c), and dT/dt refers to the diabatic cooling. By examining the individual contributions to the dq_s/dt, we find that the variations of ω and dq_s/dT can explain the patterns of the large-scale condensation term. Over the sea ice, both the lack of large-scale ascent and low temperature (smaller dq_s/dT via Clausius-Clapeyron scaling) (Figs. 13a,d) significantly lower the large-scale condensational rate of l near the surface (Fig. 11b), causing optically thin stratus over the ice packs. Likewise, it is straightforward to explain the advection dependence of l using the different patterns of ω (Figs. 13b,e) and dq_s/dT (Figs. 13e,f) associated with different advection conditions.

c. *Seasonal dependence*

So far, we have been focusing on the wintertime clouds. Does the finding of contrasting LLC regimes across the sea ice edges hold in other seasons? Figures 14 and 15 show the budgets of cloud fraction and l in other seasons. In spring and autumn, the overall patterns of cloud properties and their budgets are similar to those in winter, except for smaller magnitudes of supersaturation adjustment (or boundary layer condensation) over the transitional region. This, however, is not the case in summer when the contrasting LLC regimes between open water and sea ice disappear. In other words, the footprints of the surface type on the LLCs no longer exist in summer.

What are the physical mechanisms behind the summertime indifference of LLC regimes between the contrasting surface types? We answer this question using the idea from Kay and Gettelman (2009), who explain the weak surface dependence of summertime clouds from the perspective of atmosphere–surface decoupling. In summer, the temperature of the lower troposphere rises rapidly by absorbing solar radiation. In the ocean adjacent to the sea ice packs, however, the T_{sfc} only increases slightly (Fig. 16a) due to the large heat capacity of the ocean. Such a top-heavy heating substantially stabilizes the lower troposphere, as seen from the stronger lower

Unauthenticated | Downloaded 12/19/22 09:10 PM UTC

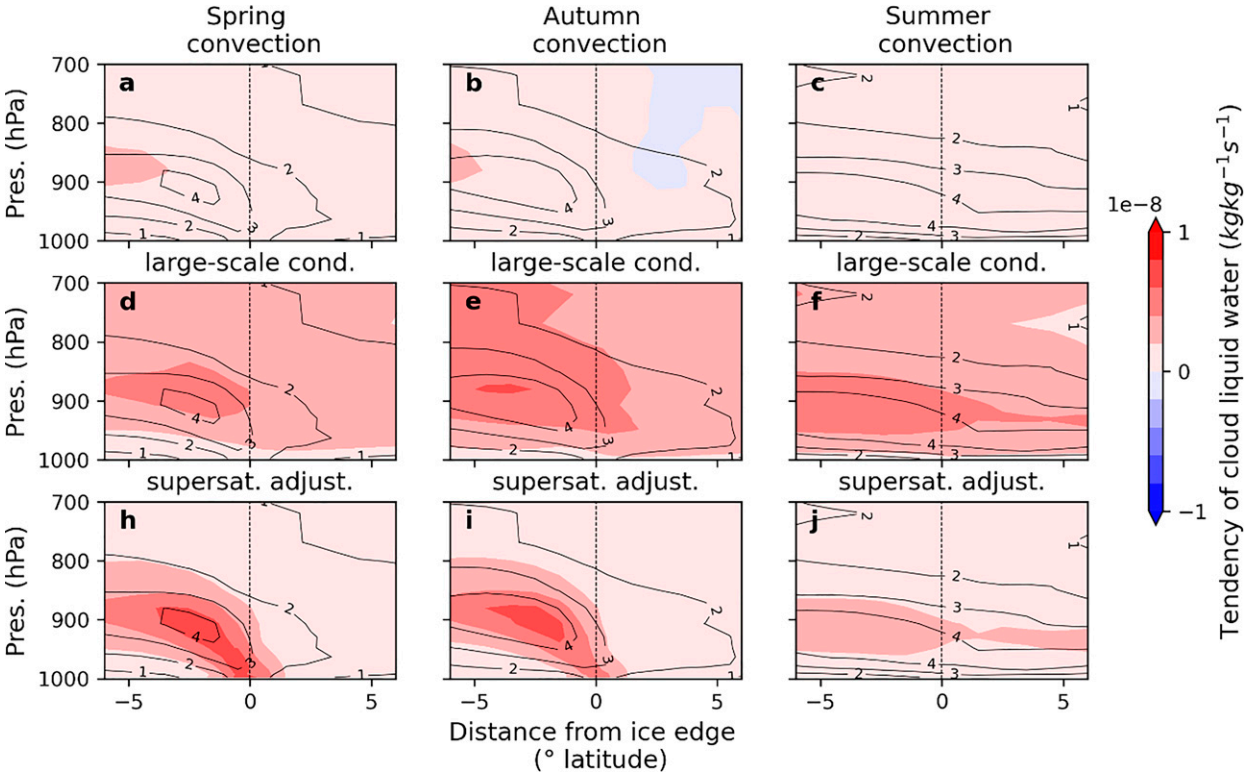


FIG. 15. As in Fig. 12, but for different seasons: (left) spring, (center) autumn, and (right) summer.

tropospheric stability (Fig. 16b) and smaller $T_{sfc} - T_a$ over the open water in summer (Fig. 16c), in which the T_a is the near-surface atmospheric temperature. The small $T_{sfc} - T_a$ suppresses the surface fluxes (Fig. 16d), disconnecting the atmosphere from the ocean, which reduces the footprints of surface type on the atmospheric processes. This decoupling argument is further supported by the limited contributions from the convection and supersaturation adjustment, two processes primarily driven by surface forcing, to the low cloud formations (Figs. 14 and 15).

5. Representativeness of the results

The analyses focus on specific regions of the Arctic and Antarctic. One might ask how representative these regions are. For example, the Atlantic Ocean part of the Arctic has many cyclones that can bring more clouds over the sea ice edge than other parts of the Arctic. To examine the representativeness of the results, we analyzed different regions: one is the Chukchi Sea and East Siberian Sea of the Arctic in autumn and the other is the Ross Sea of the Antarctic in winter (Fig. S10). The results, both from observations and cloud budget simulations, still hold (see Figs. S10–S16).

6. Discussion and conclusions

We use a climate model with a fully prognostic cloud scheme, GFDL AM4.0, to understand processes controlling polar low-level clouds (LLCs) and their changes across sea ice edges. We first evaluate the model by comparing the simulated cloud fraction, processed by a satellite simulator, with the observation from the CALIOP onboard the *CALIPSO* satellite. The comparisons were conducted not only for the mean climatology but also for processes at shorter time scales, namely the intrusions of warm and moist air (on-ice flow) and cold air outbreaks (off-ice flow). The evaluation demonstrates that the GFDL AM4.0 is skillful at reproducing the observed polar LLCs and their changes across sea ice edges.

Having demonstrated the fidelity of the AM4.0, we use the model to elucidate the mechanisms controlling the surface type dependence of polar LLCs. We examine the budgets of cloud fraction and cloud water content in a two-dimensional space with axes of height and the meridional distance to sea ice edges. The budget analyses help us address the three questions posed at the beginning of section 4.

a. What determines the climatological difference of LLCs between open water and sea ice?

Over the sea ice, the LLCs are lower and substantially thinner than those over the adjacent open waters. The difference is caused by the different mechanisms by which LLCs are formed and maintained. LLCs over sea ice are formed by large-scale condensation: the ice surface loses thermal energy to the space, cooling the near-surface air to condensation. The cloud condensates are tenuous because of the low temperature and large-scale subsidence, both suppressing the condensation rate. In contrast, maritime LLCs are sustained

Unauthenticated | Downloaded 12/19/22 09:10 PM UTC

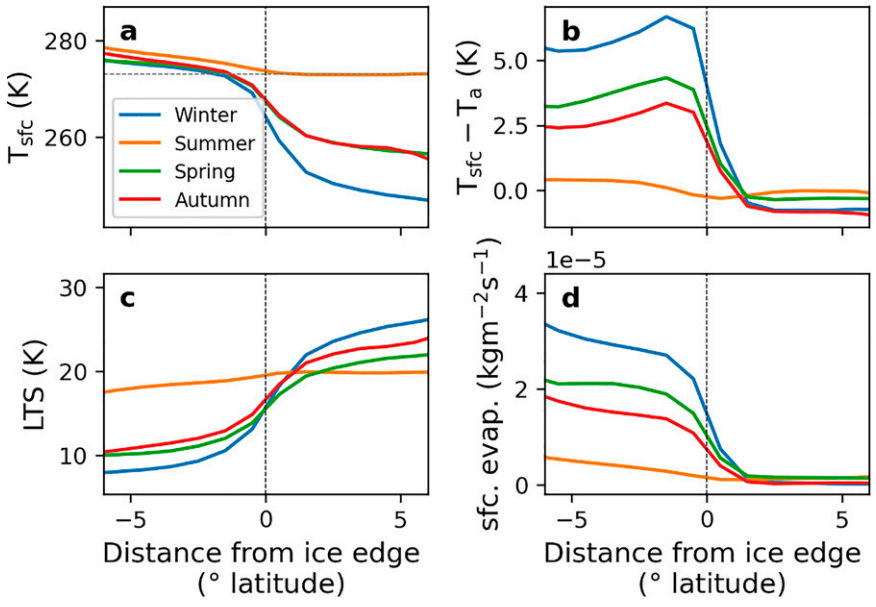


FIG. 16. AM4-modeled (a) surface temperature, (b) surface temperature minus near-surface atmospheric temperature, (c) lower tropospheric stability, and (d) surface moisture flux as a function of distance from sea ice edge for different seasons. The horizontal gray dashed line in (a) marks the freezing temperature of 273 K. The lower tropospheric stability is calculated as the potential temperature difference between the 700-hPa level and the surface (Wood and Bretherton 2006).

by not only large-scale condensation but also by convection and boundary layer mixing, which combine to form denser clouds on top of higher boundary layers.

b. What controls the formations of LLCs when they are advected across the sea ice edges?

During on-ice flow, clouds are formed via large-scale condensation (water vapor condenses by large-scale lifting and diabatic cooling), with negligible contribution from convection because of the stable lower troposphere under warm advection conditions. During the off-ice flow, the increasingly opened ocean enhances the surface moisture flux, moistening the boundary layer, which forms stratiform LLCs. Farther downstream, as the boundary layer becomes more convective, the convective detrainment dominates the sources of LLC fraction and water content.

c. Are these findings seasonally dependent?

These results hold for nonsummer seasons. In summer, the solar insolation warms the atmosphere at a much faster rate than it warms the surface. This top-heavy warming decouples the atmosphere from the surface. The decoupling significantly reduces the footprints of the surface type on the clouds, allowing the cloud field to disperse with limited modifications by the changing surface types.

This work provides further evidence of the significant role of melting sea ice on thickening LLCs in nonsummer seasons, solidifying the consensus on the positive low cloud feedback in polar regions. More importantly, we show contrasting LLC regimes between frozen and unfrozen parts of polar oceans. This finding suggests the caveat of previous studies that consider the polar LLCs as a whole, without separating the different LLC regimes. Thus, this work can motivate future research that builds upon this concept of contrasting LLC regimes to further elucidate the mechanism of the polar low cloud feedback.

Acknowledgments. Leo Donner and Nadir Jeevanjee are acknowledged for their comments and suggestions on an internal review of the manuscript. We thank Ming Zhao, Zhihong Tan, and Mitch Bushuk for the discussions. YZ thanks Pu Lin and Wenhao Dong for technical assistance. We thank Patrick Taylor and two anonymous reviewers for their constructive comments. We acknowledge GFDL resources made available for this research.

Data availability statement. The *CALIPSO*-GOCCP dataset is obtained from https://climserv.ipsl.polytechnique.fr/cfmip-obs/. The NOAA NSIDC data are from the National Snow and Ice Data Center (https://nsidc.org/data/G02202#). The reanalysis data are collected from the NCAR Research Data Archive (rda.ucar.edu/datasets/ds083.2/). Codes used to reproduce the results are available at https://github.com/youtongzheng/Zheng_Ming_2022_JCli.

REFERENCES

Anderson, J. L., and Coauthors, 2004: The new GFDL global atmosphere and land model AM2–LM2: Evaluation with prescribed SST simulations. *J. Climate*, **17**, 4641–4673, https://doi.org/10.1175/JCLI-3223.1.

Unauthenticated | Downloaded 12/19/22 09:10 PM UTC

Barton, N. P., S. A. Klein, J. S. Boyle, and Y. Y. Zhang, 2012: Arctic synoptic regimes: Comparing domain-wide Arctic cloud observations with CAM4 and CAM5 during similar dynamics. *J. Geophys. Res.*, **117**, D15205, https://doi.org/10.1029/2012JD017589.

Bretherton, C. S., and M. C. Wyant, 1997: Moisture transport, lower-tropospheric stability, and decoupling of cloud-topped boundary layers. *J. Atmos. Sci.*, **54**, 148–167, https://doi.org/10.1175/1520-0469(1997)054<0148:MTLTSA>2.0.CO;2.

Chepfer, H., S. Bony, D. Winker, G. Cesana, J. L. Dufresne, P. Minnis, C. J. Stubenrauch, and S. Zeng, 2010: The GCM-Oriented CALIPSO Cloud Product (CALIPSO-GOCCP). *J. Geophys. Res.*, **115**, D00H16, https://doi.org/10.1029/2009JD012251.

Chung, D., G. Matheou, and J. Teixeira, 2012: Steady-state large-eddy simulations to study the stratocumulus to shallow cumulus cloud transition. *J. Atmos. Sci.*, **69**, 3264–3276, https://doi.org/10.1175/JAS-D-11-0256.1.

Cronin, T. W., and E. Tziperman, 2015: Low clouds suppress Arctic air formation and amplify high-latitude continental winter warming. *Proc. Natl. Acad. Sci. USA*, **112**, 11 490–11 495, https://doi.org/10.1073/pnas.1510937112.

——, H. Li, and E. Tziperman, 2017: Suppression of Arctic air formation with climate warming: Investigation with a two-dimensional cloud-resolving model. *J. Atmos. Sci.*, **74**, 2717–2736, https://doi.org/10.1175/JAS-D-16-0193.1.

Curry, J., 1983: On the formation of continental polar air. *J. Atmos. Sci.*, **40**, 2278–2292, https://doi.org/10.1175/1520-0469(1983)040<2278:OTFOCP>2.0.CO;2.

——, J. L. Schramm, W. B. Rossow, and D. Randall, 1996: Overview of Arctic cloud and radiation characteristics. *J. Climate*, **9**, 1731–1764, https://doi.org/10.1175/1520-0442(1996)009<1731:OOACAR>2.0.CO;2.

Eastman, R., and S. G. Warren, 2010: Interannual variations of Arctic cloud types in relation to sea ice. *J. Climate*, **23**, 4216–4232, https://doi.org/10.1175/2010JCLI3492.1.

Geerts, B., 2019: Cold-Air Outbreaks in the Marine Boundary Layer Experiment (COMBLE) science implementation plan. Tech. Rep. DOE/SC-ARM-19-002, 38 pp., https://doi.org/10.2172/1499128.

Gettelman, A., and H. Morrison, 2015: Advanced two-moment bulk microphysics for global models. Part I: Off-line tests and comparison with other schemes. *J. Climate*, **28**, 1268–1287, https://doi.org/10.1175/JCLI-D-14-00102.1.

Guo, H., Y. Ming, S. Fan, L. Zhou, L. Harris, and M. Zhao, 2021: Two-moment bulk cloud microphysics with prognostic precipitation in GFDL's Atmosphere Model AM4.0: Configuration and performance. *J. Adv. Model. Earth Syst.*, **13**, e2020MS002453, https://doi.org/10.1029/2020MS002453.

Guo, Z., M. Wang, Y. Peng, and Y. Luo, 2020: Evaluation on the vertical distribution of liquid and ice phase cloud fraction in Community Atmosphere Model version 5.3 using spaceborne lidar observations. *Earth Space Sci.*, **7**, e2019EA001029, https://doi.org/10.1029/2019EA001029.

Hall, A., 2004: The role of surface albedo feedback in climate. *J. Climate*, **17**, 1550–1568, https://doi.org/10.1175/1520-0442(2004)017<1550:TROSAF>2.0.CO;2.

Herman, G., and R. Goody, 1976: Formation and persistence of summertime Arctic stratus clouds. *J. Atmos. Sci.*, **33**, 1537–1553, https://doi.org/10.1175/1520-0469(1976)033<1537:FAPOSA>2.0.CO;2.

——, and W. T. Johnson, 1980: Arctic and Antarctic climatology of a GLAS general circulation model. *Mon. Wea. Rev.*, **108**, 1974–1991, https://doi.org/10.1175/1520-0493(1980)108<1974:AAACOA>2.0.CO;2.

Hong, Y., and G. Liu, 2015: The characteristics of ice cloud properties derived from CloudSat and *CALIPSO* measurements. *J. Climate*, **28**, 3880–3901, https://doi.org/10.1175/JCLI-D-14-00666.1.

Hu, Z., T. W. Cronin, and E. Tziperman, 2018: Suppression of cold weather events over high-latitude continents in warm climates. *J. Climate*, **31**, 9625–9640, https://doi.org/10.1175/JCLI-D-18-0129.1.

Inoue, J., J. Liu, J. O. Pinto, and J. A. Curry, 2006: Intercomparison of Arctic regional climate models: Modeling clouds and radiation for SHEBA in May 1998. *J. Climate*, **19**, 4167–4178, https://doi.org/10.1175/JCLI3854.1.

Jakob, C., and S. A. Klein, 2000: A parametrization of the effects of cloud and precipitation overlap for use in general-circulation models. *Quart. J. Roy. Meteor. Soc.*, **126**, 2525–2544, https://doi.org/10.1002/qj.49712656809.

Kalnay, E., and Coauthors, 1996: The NCEP/NCAR 40-Year Reanalysis Project. *Bull. Amer. Meteor. Soc.*, **77**, 437–472, https://doi.org/10.1175/1520-0477(1996)077<0437:TNYRP>2.0.CO;2.

Kay, J. E., and A. Gettelman, 2009: Cloud influence on and response to seasonal Arctic sea ice loss. *J. Geophys. Res.*, **114**, D18204, https://doi.org/10.1029/2009JD011773.

Klein, S. A., and D. L. Hartmann, 1993: The seasonal cycle of low stratiform clouds. *J. Climate*, **6**, 1587–1606, https://doi.org/10.1175/1520-0442(1993)006<1587:TSCOLS>2.0.CO;2.

LeMone, M. A., and Coauthors, 2019: 100 years of progress in boundary layer meteorology. *A Century of Progress in Atmospheric and Related Sciences: Celebrating the American Meteorological Society Centennial, Meteor. Monogr.*, No. 59, Amer. Meteor. Soc., 9.1–9.85, https://doi.org/10.1175/AMSMONOGRAPHS-D-18-0013.1.

Lin, S.-J., 2004: A "vertically Lagrangian" finite-volume dynamical core for global models. *Mon. Wea. Rev.*, **132**, 2293–2307, https://doi.org/10.1175/1520-0493(2004)132<2293:AVLFDC>2.0.CO;2.

Lock, A. P., A. R. Brown, M. R. Bush, G. M. Martin, and R. N. B. Smith, 2000: A new boundary layer mixing scheme. Part I: Scheme description and single-column model tests. *Mon. Wea. Rev.*, **128**, 3187–3199, https://doi.org/10.1175/1520-0493(2000)128<3187:ANBLMS>2.0.CO;2.

Maloney, E. D., and Coauthors, 2019: Process-oriented evaluation of climate and weather forecasting models. *Bull. Amer. Meteor. Soc.*, **100**, 1665–1686, https://doi.org/10.1175/BAMS-D-18-0042.1.

Manabe, S., and R. T. Wetherald, 1975: The effects of doubling the CO_2 concentration on the climate of a general circulation model. *J. Atmos. Sci.*, **32**, 3–15, https://doi.org/10.1175/1520-0469(1975)032<0003:TEODTC>2.0.CO;2.

Messori, G., C. Woods, and R. Caballero, 2018: On the drivers of wintertime temperature extremes in the high Arctic. *J. Climate*, **31**, 1597–1618, https://doi.org/10.1175/JCLI-D-17-0386.1.

Monroe, E. E., P. C. Taylor, and L. N. Boisvert, 2021: Arctic cloud response to a perturbation in sea ice concentration: The North Water Polynya. *J. Geophys. Res. Atmos.*, **126**, e2020JD034409, https://doi.org/10.1029/2020JD034409.

Morrison, A. L., J. E. Kay, H. Chepfer, R. Guzman, and V. Yettella, 2018: Isolating the liquid cloud response to recent Arctic sea ice variability using spaceborne lidar observations.

Unauthenticated | Downloaded 12/19/22 09:10 PM UTC

J. Geophys. Res. Atmos., **123**, 473–490, https://doi.org/10.1002/2017JD027248.

——, ——, W. R. Frey, H. Chepfer, and R. Guzman, 2019: Cloud response to Arctic sea ice loss and implications for future feedback in the CESM1 climate model. *J. Geophys. Res. Atmos.*, **124**, 1003–1020, https://doi.org/10.1029/2018JD029142.

Morrison, H., and A. Gettelman, 2008: A new two-moment bulk stratiform cloud microphysics scheme in the Community Atmosphere Model, version 3 (CAM3). Part I: Description and numerical tests. *J. Climate*, **21**, 3642–3659, https://doi.org/10.1175/2008JCLI2105.1.

Palm, S. P., S. T. Strey, J. Spinhirne, and T. Markus, 2010: Influence of Arctic sea ice extent on polar cloud fraction and vertical structure and implications for regional climate. *J. Geophys. Res.*, **115**, D21209, https://doi.org/10.1029/2010JD013900.

Peng, G., W. N. Meier, D. J. Scott, and M. H. Savoie, 2013: A long-term and reproducible passive microwave sea ice concentration data record for climate studies and monitoring. *Earth Syst. Sci. Data*, **5**, 311–318, https://doi.org/10.5194/essd-5-311-2013.

Pithan, F., and T. Mauritsen, 2014: Arctic amplification dominated by temperature feedbacks in contemporary climate models. *Nat. Geosci.*, **7**, 181–184, https://doi.org/10.1038/ngeo2071.

Rotstayn, L. D., 1997: A physically based scheme for the treatment of stratiform clouds and precipitation in large-scale models. I: Description and evaluation of the microphysical processes. *Quart. J. Roy. Meteor. Soc.*, **123**, 1227–1282, https://doi.org/10.1002/qj.49712354106.

Schubert, W. H., J. S. Wakefield, E. J. Steiner, and S. K. Cox, 1979: Marine stratocumulus convection. Part II: Horizontally inhomogeneous solutions. *J. Atmos. Sci.*, **36**, 1308–1324, https://doi.org/10.1175/1520-0469(1979)036<1308:MSCPIH>2.0.CO;2.

Simmonds, I., 2015: Comparing and contrasting the behaviour of Arctic and Antarctic sea ice over the 35 year period 1979–2013. *Ann. Glaciol.*, **56**, 18–28, https://doi.org/10.3189/2015AoG69A909.

Stephens, G., D. Winker, J. Pelon, C. Trepte, D. Vane, C. Yuhas, T. L'Ecuyer, and M. Lebsock, 2017: *CloudSat* and *CALIPSO* within the A-Train: Ten years of actively observing the Earth system. *Bull. Amer. Meteor. Soc.*, **99**, 569–581, https://doi.org/10.1175/BAMS-D-16-0324.1.

Stroeve, J. C., M. C. Serreze, M. M. Holland, J. E. Kay, J. Malanik, and A. P. Barrett, 2012: The Arctic's rapidly shrinking sea ice cover: A research synthesis. *Climatic Change*, **110**, 1005–1027, https://doi.org/10.1007/s10584-011-0101-1.

Taylor, P. C., S. Kato, K.-M. Xu, and M. Cai, 2015: Covariance between Arctic sea ice and clouds within atmospheric state regimes at the satellite footprint level. *J. Geophys. Res. Atmos.*, **120**, 12 656–12 678, https://doi.org/10.1002/2015JD023520.

——, B. M. Hegyi, R. C. Boeke, and L. N. Boisvert, 2018: On the increasing importance of air–sea exchanges in a thawing Arctic: A review. *Atmosphere*, **9**, 41, https://doi.org/10.3390/atmos9020041.

Tiedtke, M., 1993: Representation of clouds in large-scale models. *Mon. Wea. Rev.*, **121**, 3040–3061, https://doi.org/10.1175/1520-0493(1993)121<3040:ROCILS>2.0.CO;2.

Tjernström, M., and Coauthors, 2015: Warm-air advection, air mass transformation and fog causes rapid ice melt. *Geophys. Res. Lett.*, **42**, 5594–5602, https://doi.org/10.1002/2015GL064373.

Vavrus, S., 2004: The impact of cloud feedbacks on Arctic climate under greenhouse forcing. *J. Climate*, **17**, 603–615, https://doi.org/10.1175/1520-0442(2004)017<0603:TIOCFO>2.0.CO;2.

——, D. Waliser, A. Schweiger, and J. Francis, 2008: Simulations of 20th and 21st century Arctic cloud amount in the global climate models assessed in the IPCC AR4. *Climate Dyn.*, **33**, 1099–1115, https://doi.org/10.1007/s00382-008-0475-6.

——, U. S. Bhatt, and V. A. Alexeev, 2011: Factors influencing simulated changes in future Arctic cloudiness. *J. Climate*, **24**, 4817–4830, https://doi.org/10.1175/2011JCLI4029.1.

Wall, C. J., T. Kohyama, and D. L. Hartmann, 2017: Low-cloud, boundary layer, and sea ice interactions over the Southern Ocean during winter. *J. Climate*, **30**, 4857–4871, https://doi.org/10.1175/JCLI-D-16-0483.1.

Winker, D. M., W. H. Hunt, and M. J. McGill, 2007: Initial performance assessment of CALIOP. *Geophys. Res. Lett.*, **34**, L19803, https://doi.org/10.1029/2007GL030135.

Wood, R., 2012: Stratocumulus clouds. *Mon. Wea. Rev.*, **140**, 2373–2423, https://doi.org/10.1175/MWR-D-11-00121.1.

——, and C. S. Bretherton, 2006: On the relationship between stratiform low cloud cover and lower-tropospheric stability. *J. Climate*, **19**, 6425–6432, https://doi.org/10.1175/JCLI3988.1.

Woods, C., R. Caballero, and G. Svensson, 2013: Large-scale circulation associated with moisture intrusions into the Arctic during winter. *Geophys. Res. Lett.*, **40**, 4717–4721, https://doi.org/10.1002/grl.50912.

You, C., M. Tjernström, and A. Devasthale, 2021: Warm-air advection over melting sea-ice: A Lagrangian case study. *Bound.-Layer Meteor.*, **179**, 99–116, https://doi.org/10.1007/s10546-020-00590-1.

Yu, Y., P. C. Taylor, and M. Cai, 2019: Seasonal variations of Arctic low-level clouds and its linkage to sea ice seasonal variations. *J. Geophys. Res. Atmos.*, **124**, 12 206–12 226, https://doi.org/10.1029/2019JD031014.

Zelinka, M. D., S. A. Klein, K. E. Taylor, T. Andrews, M. J. Webb, J. M. Gregory, and P. M. Forster, 2013: Contributions of different cloud types to feedbacks and rapid adjustments in CMIP5. *J. Climate*, **26**, 5007–5027, https://doi.org/10.1175/JCLI-D-12-00555.1.

Zhao, M., and Coauthors, 2018: The GFDL Global Atmosphere and Land Model AM4.0/LM4.0: 2. Model description, sensitivity studies, and tuning strategies. *J. Adv. Model. Earth Syst.*, **10**, 735–769, https://doi.org/10.1002/2017MS001209.

Zheng, Y., and Z. Li, 2019: Episodes of warm-air advection causing cloud-surface decoupling during the MARCUS. *J. Geophys. Res. Atmos.*, **124**, 12 227–12 243, https://doi.org/10.1029/2019JD030835.

——, D. Rosenfeld, and Z. Li, 2018: Estimating the decoupling degree of subtropical marine stratocumulus decks from satellite. *Geophys. Res. Lett.*, **45**, 12 560–12 568, https://doi.org/10.1029/2018GL078382.

——, ——, and ——, 2020: A more general paradigm for understanding the decoupling of stratocumulus-topped boundary layers: The importance of horizontal temperature advection. *Geophys. Res. Lett.*, **47**, e2020GL087697, https://doi.org/10.1029/2020GL087697.

Zhou, X., P. Kollias, and E. R. Lewis, 2015: Clouds, precipitation, and marine boundary layer structure during the MAGIC field campaign. *J. Climate*, **28**, 2420–2442, https://doi.org/10.1175/JCLI-D-14-00320.1.

Unauthenticated | Downloaded 12/19/22 09:10 PM UTC